Journal of Thermal Analysis and Calorimetry (2020) 139:1637–1653
https://doi.org/10.1007/s10973-019-08562-5

Heat transfer and pressure drop investigation through pipe with different shapes using different types of nanofluids

Ali H. Abdelrazek[1] · S. N. Kazi[1] · Omer A. Alawi[2,3] · Nukman Yusoff[1] · Cheen Sean Oon[1] · Hafiz Muhammad Ali[4]

Received: 29 October 2018 / Accepted: 4 July 2019 / Published online: 19 July 2019

Abstract

In the present study, the heat transfer and hydrodynamic analysis of flow through single-pipe heat exchangers of circular and square cross-sectional configurations were performed. The experimental and numerical investigations were conducted to evaluate the performance of two metallic oxides (Al_2O_3 and SiO_2) and two carbon-based nanostructured nanofluids (KRG and GNP) in comparison with the distilled water (DW). The data obtained from the experimental runs with DW as a working fluid in both test sections were used to validate the 3-D numerical models for the square and circular pipe heat exchangers. The flow in both test sections is considered as a fully developed turbulent flow with the Reynolds number range of 6000–11,000, and both the test sections were subjected to a uniform heat flux at their outer surfaces. The concentrations of all nanofluids used in the present study were in the range of (0.025–0.1 mass%). The test rig was firstly validated during the water run by using different empirical correlations for the evaluation of pressure drop and Nusselt number and showing a very good agreement, and then, the numerical models were validated with the data obtained experimentally and the errors were less than 10% for both models. For the square tube flow, the average errors between the numerical and experimental findings of Nusselt number and pressure drop were 6.8% and 2.49%, respectively, and for the circular pipe flow, the evaluated errors were 9.34% and 5.92% for Nusselt number and pressure drop, respectively. The performance index for all the nanofluids was calculated to obtain the convective heat transfer coefficients and friction losses of the fluids in both the tubes. The results showed that the non-covalent graphene–DW is not suitable for heat transfer applications due to its higher viscosity. The results also showed a different enhancement of heat transfer for the same nanofluid in circular and square tube flows, whereas the performance index of the same nanofluid appears nearly the same for flow through both the cross sections.

Keywords Metallic oxides nanofluids · Carbon-based nanostructures · Heat transfer · Square tube · Circular tube · Turbulent flow

List of symbols

Al_2O_3	Aluminium oxide
A_c	Cross-sectional area (m^2)
A_s	Total heat transfer surface area (m^2)
C_f	Friction coefficient
C_p	Specific heat (kJ kg^{-1} K^{-1})

✉ Ali H. Abdelrazek
ali_hassan80@siswa.um.edu.my; ali.h.razek@outlook.com

✉ S. N. Kazi
salimnewaz@um.edu.my; salimnewaz@yahoo.com

[1] Department of Mechanical Engineering, University Malaya, 50603 Kuala Lumpur, Malaysia

[2] Department for Management of Science and Technology Development, Ton Duc Thang University, Ho Chi Minh City, Vietnam

[3] Faculty of Applied Sciences, Ton Duc Thang University, Ho Chi Minh City, Vietnam

[4] Mechanical Engineering Department, University of Engineering and Technology, Taxila 47050, Pakistan

D	Nominal diameter of circular tube (mm)
D_h	Hydraulic tube diameter [$4A_c/p$ (m)]
D_{ins}	Diameter of insulation layer (mm)
d_p	Nanoparticle diameter (μm)
DW	Distilled water
f	Friction factor
H	Head produced by the pump (m)
h	Convection heat transfer coefficient (W m^{-2} K^{-1})
I	Current (A)
K	Thermal conductivity (W m^{-1} K^{-1})
k	Turbulent kinetic energy
L	Tube computational length (mm)
L_S	Side length of square tube (m)
Nu	Nusselt number
P	Pressure (Pa)
p	Perimeter (m)
Pr	Prandtl number
q	Heat transfer rate (W)
q''	Heat flux (W m^{-2})
Re	Reynolds number
SiO_2	Silicon oxide
T	Temperature (K)
T_b	Fluid bulk temperature (K)
T_{in}	Inlet temperature (K)
T_o	Outlet temperature (K)
T_w	Tube wall temperature (K)
u	Velocity component in x direction (m s^{-1})
v	Velocity component in y direction (m s^{-1})
V	Mean flow velocity (m s^{-1})
ΔV	Voltage difference (V)
$\dot{V}$	Volume flow rate (m^3)
$\dot{W}$	Hydraulic pumping power (W)

Greek symbols

α_{th}	Thermal diffusivity of the fluid (m^2 s^{-1})
γ	Specific mass of the fluid (N m^{-3})
ε	Turbulent dissipation rate (m^2 s^{-2})
v	Momentum diffusivity or kinematic viscosity (m^2 s^{-1})
φ	Nanoparticle volume fraction (%)
μ	Dynamic viscosity (N m s^{-1})
μ_t	Eddy viscosity (N m s^{-1})
τ	Shear stress (Pa)
ρ	Density (kg m^{-3})
ω	Nanoparticle mass concentration

Subscripts

b	Bulk
bf	Base fluid
cr	Circular
in	Inlet
ins	Insulation
nf	Nanofluid
o	Outlet
s	Solid
sq	Square
t	Turbulence
th	Thermal
f	Fluid
p	Particles
w	Wall

Introduction

Nanofluids are characterized as suspensions of nanoparticles in the base fluids [1]. In general, nanofluids are a relatively new class of fluids which consists of a base fluid with suspended nanosized particles (1–100 nm). These nanoparticles are synthesized from metals (e.g. Al, Cu, Ag, and Au), metal oxides (e.g. aluminium oxide, silicon oxide, zirconium oxide), metal carbides, metal nitrides, and carbon derivatives (e.g. diamond, graphene, fullerene, and CNT), while base fluids might be distilled water or organic liquids such as different types of refrigerants, liquid fuels, lubricating oils, and ethylene–glycol [2]. Therefore, when compared to the base fluid, the changes in thermophysical properties of such mixtures occur, e.g. viscosity, specific heat, density, and thermal conductivity [3].

The use of nanofluids as heat transfer medium is limited to the fact that the thermal conductivities of the solid material particles are typically an order of magnitude higher than those of the conventional heat exchanging fluids such as water. Then, it is predictable that a suspension of nanosized solid particles in a base fluid, even at low volume concentrations, can cause a significant increase in the thermal performance [2, 4–8]. Hence, the industrial fields could be benefited from such improved heat transfer fluids as the nanofluids have the potential to reduce the thermal resistances. Study of the behaviour and nature of nanofluids is somewhat complicated as they have the characteristics of both single- and two-phase fluids. So, modelling of nanofluids with single-phase versus two-phase approach is a source of controversy among researchers for the last two decades according to [9, 10]. Pendyala et al. [9] and Vajjha et al. [10] concluded that nanofluids could be modelled with a single-phase approach as its particles are very fine and have Newtonian behaviour as the traditional fluids. So, it is acceptable to apply the classic concepts to nanofluids including conservation equations using effective thermophysical properties.

As the shapes and designs of heat exchanger pipes are different according to their applications, various numerical and experimental studies were performed on different

shapes of pipes to study the effect of using nanofluids as alternatives to the normal heat transfer fluids. Performance of heat exchangers with flat or elliptic tubes was evaluated by different authors [9–15], wavy tubes [16, 17], and annular spaces [18–24], and a number of numerical and experimental studies were conducted to obtain the performance of heat transfer and pressure drop inside square and rectangular ducts using nanofluids under different flow regimes [25–32]. All the noted studies showed a significant enhancement in heat transfer by using nanofluids as a working fluid where pressure drop was increased as well.

Despite the diversity of pipe shapes and designs, the pipes of circular cross section still considered the most common pipes used in the engineering applications. Therefore, many studies were conducted to observe the effect of using nanofluids as heat transfer medium in circular tubes, either in experimental [33–39] or numerical [40–52] mode of investigation. Those studies showed that a certain enhancement was achieved in heat transfer characteristics by using of nanofluids regardless of the parameters governing nanofluid performance, the nanoparticle concentration, types of nanoparticles, or nanoparticle size.

In heat transfer study, comparison between the effects of different shapes of pipes is very important to select the proper flow configurations for different applications according to their performance with the use of new heat transfer fluids. As the reported works in the literature are mostly limited to a single flow passage, and the comparative study between different configurations are very limited in the turbulent region, the present study has focused on the comparison between circular and square tube configurations on heat transfer and fluid flow performance inside circular and square heat exchangers under fully developed turbulent flow. Two carbon nanostructures nanofluids (KRG and GNP) and two metallic oxides nanofluids (Al_2O_3 and SiO_2) are examined. Experimental and numerical studies are performed to evaluate the characteristics of different nanofluids using different cross sections of tubes.

Methodology

Nanofluids and their thermophysical properties

A comparison between metal oxides and carbon-based nanomaterials has performed on the present study. Silica and alumina nanopowders of 13 nm diameter were purchased from Sigma-Aldrich and used to prepare the water-based nanofluids by two-step technique for three different concentrations of each of the nanopowders. The distilled water was obtained experimentally by a water still distiller of capacity 4 L h^{-1} and its thermophysical properties were measured experimentally. The SiO_2/DW and Al_2O_3/DW nanofluids were prepared with concentrations of 0.1 mass%, 0.075 mass%, and 0.05 mass% by sonicating the mixture of the nanopowder and the distilled water for 60 min to get a uniform dispersed colloid without any settlement.

Figure 1 shows the different concentrations of the SiO_2/DW and Al_2O_3/DW nanofluids after preparation during 30 days. Thus, according to the pictures captured at different days the stability of all samples is good enough to run the experiments. The thermal conductivity of DW, SiO_2/DW, and Al_2O_3/DW nanofluids was measured by using KD2 pro instrument. The viscosity of DW and nanofluids was measured using a rotational rheometer (Physica, MCR-301, Anton Paar, Graz, Austria), while the density and specific heat of nanofluids were obtained based on mixture correlations (Eqs. 1, 2)

$$\rho_{nf} = (1-\varphi_p)\rho_{bf} + \varphi_p\rho_p \tag{1}$$

$$C_{p,nf} = \frac{(1-\varphi_p)\rho_{bf}C_{bf} + \varphi_p\rho_p C_p}{\rho_{nf}}. \tag{2}$$

The volume fraction φ in Eqs. (1) and (2) is obtained from the mass percentage (mass%) concentration as shown in Eq. (3)

$$\varphi_p = \frac{\omega_p\rho_{bf}}{(100-\omega_p)\rho_p + \omega_p\rho_{bf}} \tag{3}$$

Two more water-based nanofluids were prepared from a carbon-based nanomaterial, and they were selected from the available literature. One of them is alkaline oxide of graphene (KRG) which was prepared by Ghozatloo et al. [53] with three different mass concentrations (0.1 mass%, 0.075 mass%, and 0.05 mass%), and the second one is a non-covalent GNP nanofluid which was prepared by Arzani et al. [54] with three different mass concentrations of 0.1 mass%, 0.05 mass%, and 0.025 mass%. Table 1 shows the effective thermophysical properties of different nanofluids.

Experimental

Figure 2 shows the test rig used in the current investigation; the experimental setup consists of the main flow loop with bypass lines which consists of the flow controlling valves, Araki EX-70R magnetic pump of maximum capacity 88 L minAl_2O_3 and zero discharge head of 6.8 m, pressure gauge, Bürkert Contromatic SE 32 inline paddle wheel flowmeter, 10-L capacity jacketed reservoir tank, flow piping drain lines, and two parallel test sections with different geometries, and a set of hand-operated gate valves were used to switch the flow between test sections. To control the temperature inside the nanofluid tank, a 2.2 kW capacity chiller was used to control the temperature of the

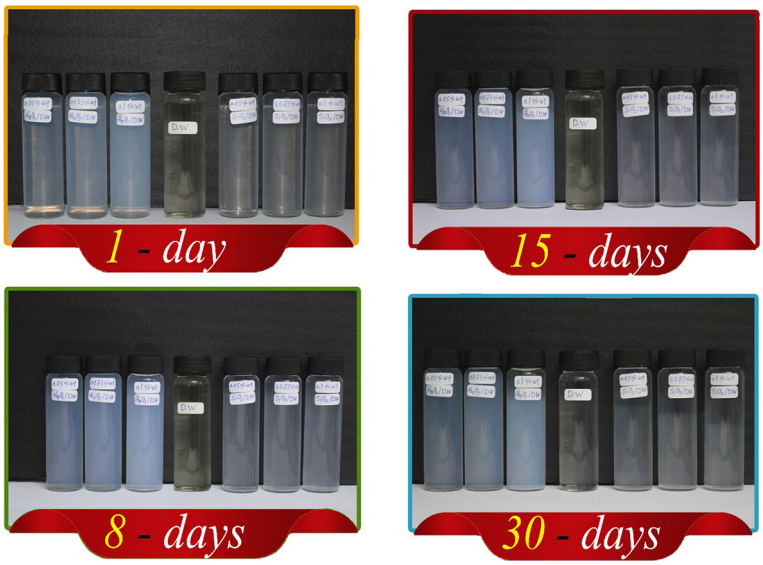

Fig. 1 Dispersion stability of Al_2O_3/DW and SiO_2/DW samples during 30 days

Table 1 Effective thermophysical properties of nanofluids concentrations at 30 °C

Fluid	μ/Pa s	ρ/kg m^{-3}	C_p/J kg^{-1} K^{-1}	K/W m^{-1} K^{-1}	α_{th}/m^2 s^{-1}	ν/m^2 s^{-1}
DW	8.51E−04	995.1731	4070.2	0.603	1.48869E−07	8.55E−07
Al_2O_3/DW						
(0.1 mass%)	(9.45E−04)	(995.7489)	(4067.649)	(0.627)	1.54697E−07	9.50E−07
(0.075 mass%)	(9.30E−04)	(995.6049)	(4068.287)	(0.619)	1.52938E−07	9.34E−07
(0.05 mass%)	(8.81E−04)	(995.4609)	(4068.925)	(0.607)	1.49873E−07	8.85E−07
SiO_2/DW						
(0.1 mass%)	(9.50E−04)	(995.4102)	(4068.764)	(0.616)	1.52012E−07	9.55E−07
(0.075 mass%)	(9.30E−04)	(995.3509)	(4069.124)	(0.606)	1.49713E−07	9.34E−07
(0.05 mass%)	(9.01E−04)	(995.2926)	(4069.482)	(0.604)	1.49072E−07	9.05E−07
KRG/DW [53]						
(0.1 mass%)	(9.977E−04)	(1053.5)	(3840.1)	(0.689)	1.70311E−07	9.47E−07
(0.075 mass%)	(9.698E−04)	(1038.4)	(3924.9)	(0.791)	1.94081E−07	9.34E−07
(0.05 mass%)	(9.429E−04)	(1023.8)	(4009.4)	(0.704)	1.71506E−07	9.21E−07
GNP–SDBS/DW [54]						
(0.1 mass%)	(0.0013)	(998.158)	(4055.95)	(0.695)	1.71669E−07	1.30E−06
(0.05 mass%)	(0.0011)	(996.889)	(4104.075)	(0.675)	1.64984E−07	1.10E−06
(0.025 mass%)	(0.0010)	(995.115)	(4152.66)	(0.645)	1.56085E−07	1.00E−06

water flowing through the jacketed space of the nanofluid tank. A pressure transducer (PX154-025DI made by OMEGA) of accuracy ± 0.75% was used to measure the pressure drop through the test section and digital data logger, and (GRAPHTECH midi logger GL 220) was connected to five *k*-type thermocouples (of accuracy ± 0.1 °C) measuring the surface temperatures of each of the test sections. The two parallel test sections were a straight stainless steel tube of the same inside hydraulic diameter of 10 mm: one with circular cross section and the other with square cross section. Both the test sections were 1400 mm length, and each of them had five equally spaced thermocouples on its surface and two RTD sensors (PT 100) to measure the bulk temperatures of the flow at the inlet and outlet. Both the test sections were specially built to retard the axial heat flow along the axial flow direction by introducing Teflon fittings at both ends. Figure 3 shows different sectional views for the test sections, and the entrance region of both the test sections was 120 mm long to confirm a fully developed flow through the heated

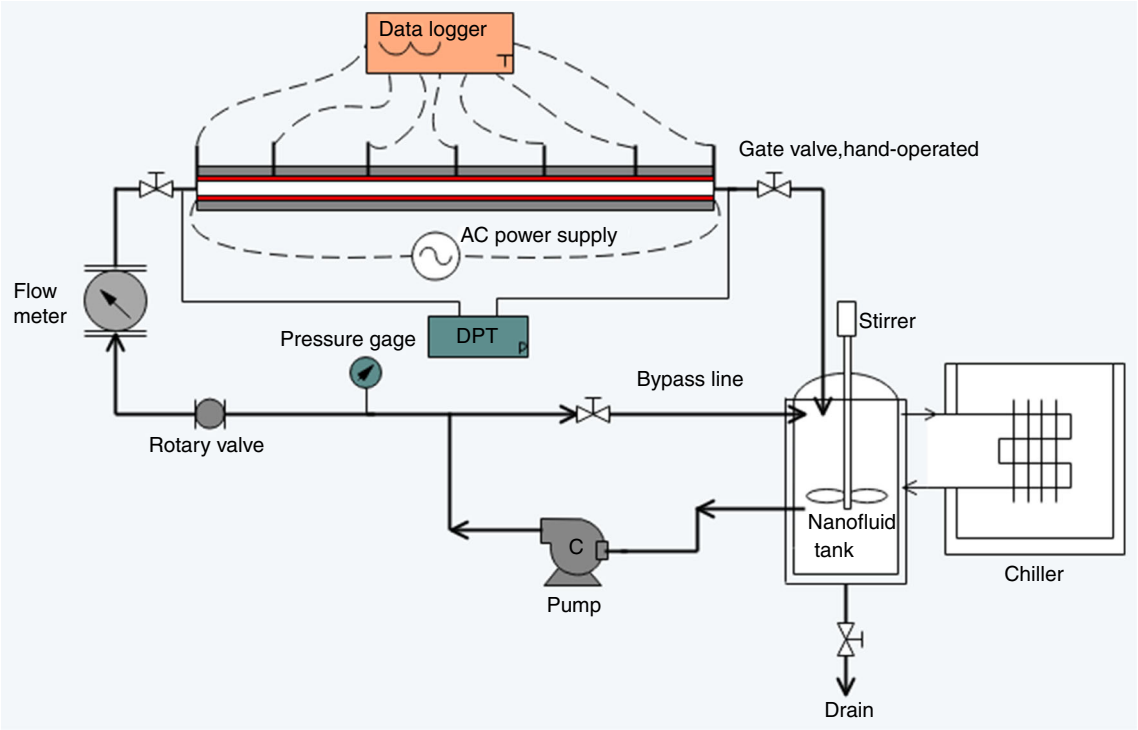

Fig. 2 Experimental setup for pipe flow with different geometric configurations

section. The heated section was wrapped carefully with an electrical tape heating element of 900 W maximum power capacity to provide a uniform heat flux along the circumference, and the input electrical power was controlled by a variable voltage transformer. To minimize the heat loss from the heater to the surroundings, a thick layer of glass wool was used as an insulation and covered from outside with a bright aluminium foil sheet. In this experimental observation, nanofluid was pumped from the tank through the test section at different pump speeds controlled by a motor speed regulating inverter which produced different flow rates. In each flow rate, the heat flux was kept constant by using a variable voltage transformer which implements heat transfer approach of constant heat flux. The inlet temperature at the test section in all the cases was kept constant by an auto-control chiller. All the data were recorded from the Graphtec data logger display and analysed in a spreadsheet.

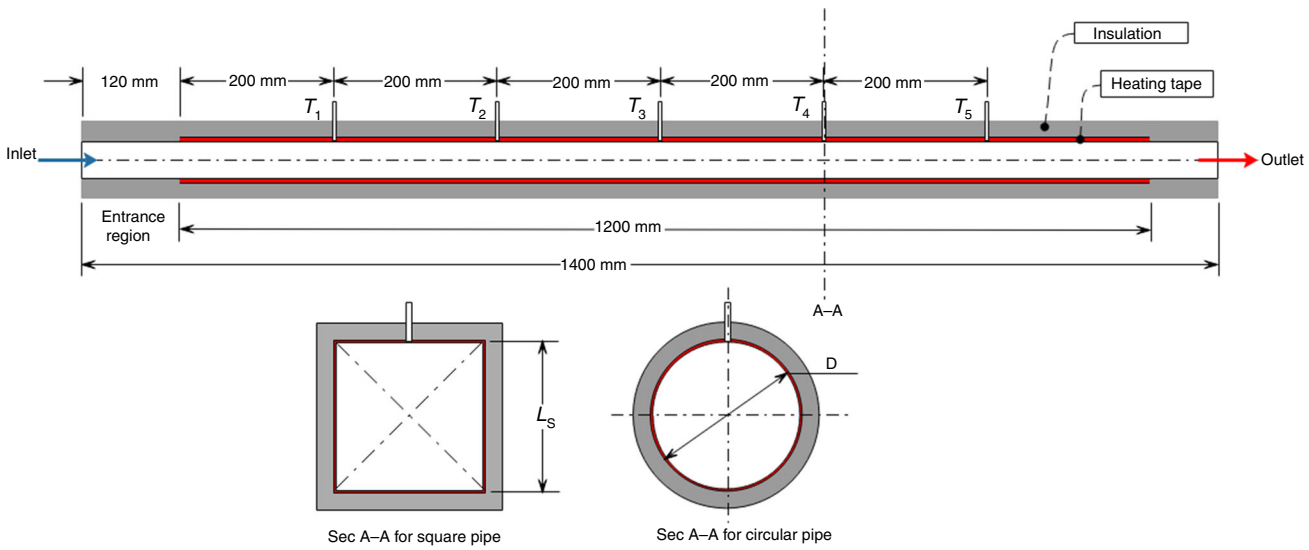

Fig. 3 Sectional view of test sections with different cross sections

Formulation of pressure drop and heat transfer

The value of the mean velocity through the circular and square cross-sectional pipes was determined by using Eq. (4):

$$V = \frac{Re\mu}{\rho D_h} \tag{4}$$

which means that the inlet flow velocity will be different for each nanofluid concentration and will have the same value for the same fluid in both ducts at different Reynolds numbers. The pumping power and pressure drop were considered as two important factors in comparison between the two geometries. The hydraulic pumping power was calculated from Eq. (5), and the volume flow rate was calculated from Eq. (6). Therefore, the volume flow rate will be different in both ducts according to the values of their cross-sectional areas

$$\dot{W} = \dot{V}\Delta P \tag{5}$$

where $\dot{W}$ is the hydraulic pumping power in W, $\dot{V}$ is the total volume flow rate in m^3, and ΔP is the total pressure drop across the pipe length in Pa

$$\begin{aligned} &\dot{V} = A_c V, \\ &A_c = {\pi D^2}/{4} \text{ for circular duct and } A_c \\ &\quad = L_S^2 \text{ for square one.} \end{aligned} \tag{6}$$

The selection of nanofluids in the industrial applications is dependent on the evaluation of heat transfer enhancement and pressure loss as well. The pressure drop through a closed conduit is calculated according to Eq. (7) [55]

$$\frac{\Delta P}{L} = 2C_f\left(\frac{\rho V^2}{D_h}\right) \tag{7}$$

where C_f is the friction coefficient or "fanning friction factor", which is calculated from Eq. (8)

$$C_f = \frac{\tau_s}{\rho V^2/2} \tag{8}$$

where τ_s is the wall shear stress, V is the average flow velocity, and the friction coefficient $C_f = {f}/{4}$ where f is the friction factor.

The average convective heat transfer coefficient is calculated from Newton's law for cooling as shown in Eq. (9)

$$h = \frac{q''}{(T_w - T_b)} \tag{9}$$

where q'' is the total heat flux, T_w is the average temperature of inner wall surface, and T_b is the average bulk temperature of the fluid and it is equals to the mean value of inlet and outlet temperatures, where the outlet temperature for both tubes can be calculated as per Eq. (10)

$$q = q''A_s = \rho\dot{V}C_p(T_o - T_{in}) \rightarrow T_o = \frac{q''A_s}{\rho\dot{V}C_p} + T_{in} \tag{10}$$

where A_s is the total heat transfer surface area, and the average Nusselt number can be evaluated as shown in Eq. (11)

$$Nu = \frac{D_h}{K}\frac{q''}{(T_w - T_b)} \tag{11}$$

To calculate the uncertainty of the experimental output data such as Reynolds number, Nusselt number, convection heat transfer coefficient, and friction factor, Eq. (12) presented by Taylor and Thompson [56] is applied

$$U_R = \left[\sum_{i=1}^{n}\left(\frac{\partial R}{\partial V_i}U_{V_i}\right)^2\right]^{0.5} \tag{12}$$

where U_R and U_{V_i} are the uncertainties associated with the parameters R and the independent variable (V_i), respectively. Moreover, n is the number of the independent variables. The uncertainty of different output data for both test section is presented in Table 2.

Mathematical formulation and numerical procedure

Governing equations

As concluded by many researchers [57, 58], the nanofluids can be treated as a homogeneous single-phase material, and therefore, the temperature and velocity field will be the same for both nanoparticles and base fluid and the effective properties of nanofluids can be used to solve the continuity, momentum, and energy equations. For 3-D physical domain with fluid of constant thermophysical properties, the conservation equations for forced turbulent flow under steady-state conditions are as follows:

Continuity equation:

$$\nabla \cdot \vec{V} = 0.0 \tag{13}$$

Momentum equation:

Table 2 Uncertainty values for the circular and the square test section

Variables	Uncertainty range %	
	Circular	Square
Reynolds number, *Re*	± 0.312	± 0.36
Convective heat transfer coefficient, *h*	± 0.801	± 1.02
Nusselt number, *Nu*	± 0.807	± 1.31
Friction factor, *f*	± 0.57	± 0.85

$$\vec{V}\left(\nabla \cdot \vec{V}\right) = \frac{1}{\rho}\left[-\nabla P + \mu \nabla^2 \vec{V} + \rho \vec{g}\right] \quad (14)$$

Energy equation:

$$\left(\nabla \cdot \vec{V}\right) T = \alpha_{\text{th}} \nabla^2 T \quad (15)$$

To solve the governing equations, in the present investigation, the $(k - \varepsilon)$ turbulent models presented by Launder and Spalding [59] is applied. The turbulent kinetic energy is calculated from Eq. (16) as follows:

$$\nabla \cdot (\rho k V) = \nabla \cdot \left[\left(\frac{\mu_t}{\sigma_k}\right) \nabla(k)\right] + G_k - \rho\varepsilon \quad (16)$$

where G_k represents the generation of turbulence kinetic energy due to mean velocity gradient and $\mu_t = \rho C_\mu {}^{k^2}/_{\varepsilon}$ is the turbulence viscosity. Specific rate of dissipation for kinetic energy, ε, for $(k - \varepsilon)$ model is presented by Eq. (17)

$$\nabla \cdot (\rho \varepsilon V) = \nabla \cdot \left[\left(\frac{\mu_t}{\sigma_\varepsilon}\right) \nabla \varepsilon\right] + \frac{\varepsilon}{k}(C_{1\varepsilon} G_k + \varepsilon C_{2\varepsilon} \rho). \quad (17)$$

The values of constants C_μ, $C_{1\varepsilon}$, $C_{2\varepsilon}$, σ_k, and σ_ε are 0.09, 1.44, 1.92, 1.0, and 1.3, respectively.

Computational domain and meshing

Figures 4 and 5 show the physical model and meshing of 3-D thin-walled horizontal tubes of circular and square cross sections, respectively. Both the tubes were with the same hydraulic diameter of 10 mm, and the heated section length was taken as the length of the tube for both the models. In the modelling process, both the tubes were considered as a solid tube with uniform constant heat flux and the heat was transferring radially towards the fluid which had a flow direction as shown in Figs. 4 and 5.

The computational grids of the circular and square models were constructed by meshing tool in ANSYS Fluent software, and the mesh in both the cases was finer near the walls because the boundary layers in this region have sharp changes. The solution of governing equation was tested at different mesh elements to validate the mesh dependency.

Numerical solution and boundary conditions

The ANSYS Fluent solver is using finite volume approach to convert the governing partial differential equations into a system of discrete algebraic equations, and then, it is solving them based on the defined boundary conditions. A realizable $(k - \varepsilon)$ model was chosen with the enhanced wall treatment for the turbulent layers adjacent to the wall and the SIMPLE scheme was chosen for pressure–velocity coupling, and the residual values were taken as $1e^{-6}$ for all computational parameters. Comparison between the two flow passage configurations according to the thermal performance should be calculated at the same boundary conditions. Therefore, the heat rate added to the wall of each duct should be the same where it produces a different heat flux on each of the wall surfaces due to the difference in the surface area between the square and circular tubes as shown in Eq. (18)

$$q = q'' A_s = q'' (\pi D L) = q'' (4 L_S L). \quad (18)$$

The boundary conditions of the experimental and the numerical solutions are the same except the values of heat fluxes added to the tube walls, and the values of the numerical solution are higher than experimental data which provide a significant enhancement in the outlet temperature. In the numerical solution, a uniform constant heat flux of 50,000 W m^{-2} is applied at the wall of the square duct, and according to Eq. (18), a 63,661.98 W m^{-2} is applied to the wall of the circular tube. The range of Reynolds number was in the range of 6000–11,000 where the thermophysical properties of fluids were considered to be constant at the inlet temperature of 30 °C.

Results and discussion

Validation and mesh dependency

The mesh dependency test was carried out for both models by evaluation of the average outlet temperature as in Eq. (10) for distilled water as a convective medium at different mesh densities. Mesh densities of 384,000, 600,000, 864,000, 1,563,000, and 2,400,000 elements were examined for the numerical solution of square duct, and mesh densities of 313,709, 583,889, 968,016, 1,337,232, and 5,476,460 elements were examined for the numerical solution of circular tube. Figure 6 shows that the numerical solution is independent of the mesh density when the number of mesh elements equal or greater than 864,000 and 1,337,232 elements for square and circular tubes, respectively. Therefore, the mesh density of 864,000 and 1337232 elements were displayed for the numerical solution of square and circular tubes, respectively.

To validate the results of the numerical solution, the experimental test rig was firstly validated for water run by comparing the measured pressure drop and the Nusselt number obtained from the experimental data with those obtained from different empirical correlations for pressure drop and Nusselt number at the same range of Reynolds numbers. The second step is the validation of the Nusselt number and pressure drop obtained numerically by

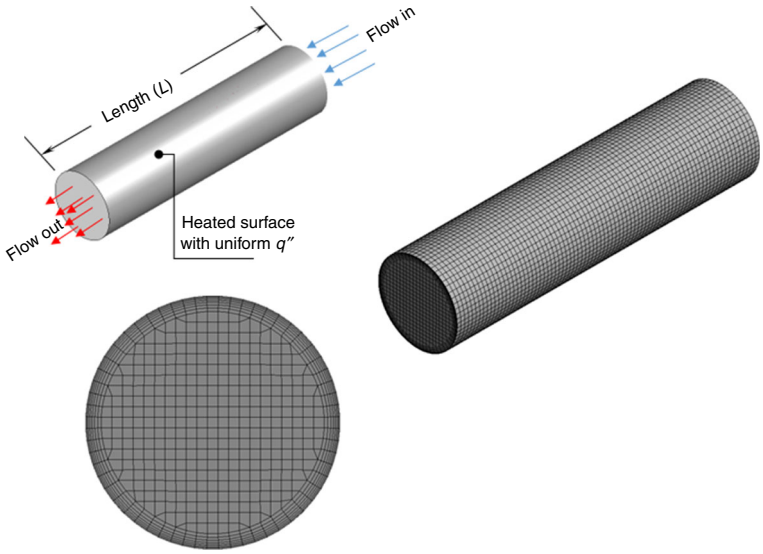

Fig. 4 Physical model and meshing of circular tube

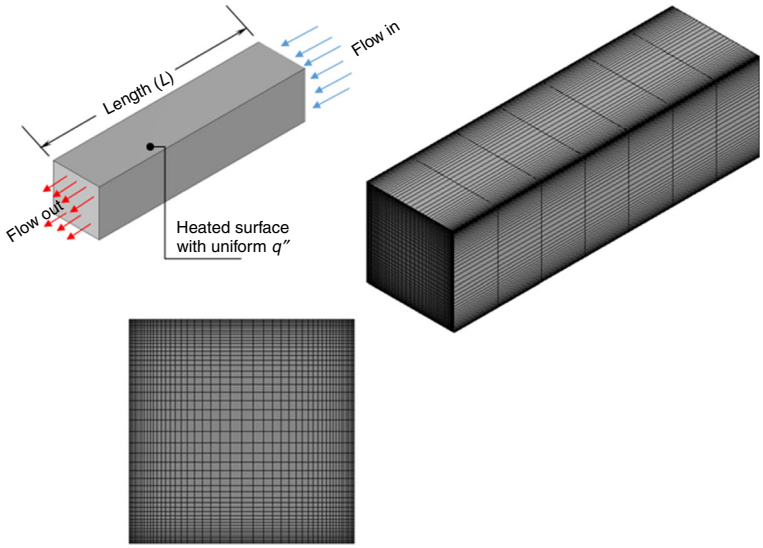

Fig. 5 Physical model and meshing of square duct

comparing them with those obtained experimentally for the water run experiment.

Gnielinski [60] presented one of the most accurate empirical correlations to calculate Nusselt number through the smooth pipe flow as shown in Eq. (19)

$$Nu = \frac{\left(\frac{f}{8}\right)(Re_{D_h} - 1000)Pr}{1 + 12.7\sqrt{f/8}\left(Pr^{2/3} - 1\right)} \tag{19}$$

where f is calculated according to Petukhov [61] and Blasius [57] correlations as shown in Eqs. (20) and (20):

$$f = (0.790 \ln Re_{Dh} - 1.64)^{-2} \tag{20}$$

$$f = 0.3164\, Re_{Dh}^{-0.25} \tag{21}$$

As discussed by Duan et al. [62], the friction factor f was calculated from Blasius correlation which should be modified for non-circular cross-sectional tubes to include the effect of geometric characteristic parameter. For tubes with square cross section, the modified Blasius friction factor will be calculated as in Eq. (22)

$$f = 0.3068\, Re_{Dh}^{-0.25}. \tag{22}$$

In the current study, the friction factor in Eq. (19) will be calculated according to Eqs. (21) and (22) for circular and square pipes because Blasius correlation is more accurate in the Re range of this study.

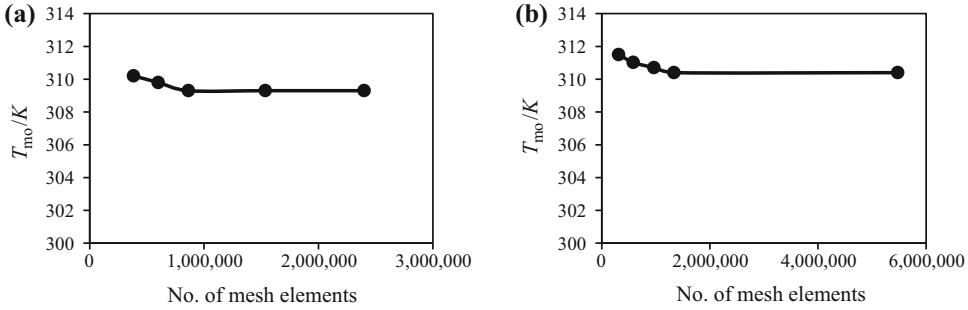

Fig. 6 Average outlet temperature at Re = 11,000 with different mesh densities: **a** square duct, **b** circular tube

The empirical correlation obtained by Dittus and Boelter [63] which is shown in Eq. (23) was used to validate the Nusselt number for pipe flow

$$Nu = 0.023Re^{0.8}Pr^{n} \tag{23}$$

where $n = 0.4$ or 0.3 in case of heating or cooling, respectively. The results of measured pressure drop were validated with the pressure drop calculated from Eq. (7), where the friction factor was calculated by Petukhov or Blasius correlation [64].

The validation curves of the experimental results for square and circular test sections are shown in Figs. 7 and 8, respectively. For the square test section, the values of Nusselt number obtained experimentally show a good agreement with those obtained from the empirical correlations of Dittus and Boelter and Gnielinski with an average error of 9.85% and 7.28%, respectively, and the average errors of the measured $\Delta P/L$ for the square test section are 6.01% and 9.59% in comparison with Petukhov and Blasius equation, respectively. For the circular test section, the Nu obtained experimentally show an average error of 2.13% and 4.82% when comparing with the empirical correlations of Dittus and Boelter and Gnielinski, respectively, and the measured $\Delta P/L$ shows a good agreement with the values obtained from the equations of Petukhov and Blasius with an average error of 8.87% and 9.13%, respectively. Also, to ensure that the percentage of heat loss to the surroundings from both the circular and square pipes has no significant effects on the heat transfer calculations, a comparative assessment was made between the input and output energy at different values of Re. The conventional energy balance equation $\left(q = I\Delta V = \rho \dot{V} C_{\mathrm{p}}(T_{\mathrm{o}} - T_{\mathrm{in}})\right)$ showed a reasonable average loss of 3.76% and 4.23% for the circular and square tubes, respectively, which would not affect the calculation of heat transfer parameters.

Figure 9 shows the comparison of the Nusselt number and pressure drop obtained numerically and those which obtained experimentally for the square and circular tubes for the water run experiments. For the square duct, the Nusselt number and pressure drop obtained numerically show a good agreement with those obtained experimentally with an average error of 6.8% and 2.49% for Nu and $\Delta P/L$, respectively. For circular tube, the average errors of Nusselt number and pressure drop were 9.34% and 5.92%, respectively. Therefore, the numerical solution obtained by the ANSYS Fluent model is accepted for both the models as average errors are in the acceptable range of less than 10%.

Thermal and flow characteristics

In this section, the thermal and fluid flow characteristics of the fluid in the circular and square tubes during the water run were discussed to investigate the suitability of the thermal and hydrodynamic features over the standard fluids. For turbulent flow, the corners with sharp edges of square tubes may create a secondary flow and Reynolds stress gradient other than the flow in the circular tubes which is more uniform and has no secondary flow as shown in Fig. 10.

Figure 11 displays the wall temperature contours for square and circular tubes exposed to uniform heat flux, where the hot temperature spots were appeared at the corners of the square duct due to the formation of the secondary flow [61]. As shown in Fig. 12, the profiles of the local Nusselt number and local friction factor were constant along the tube length of $x/D_{\mathrm{h}} \geq 10$, which satisfies the standard considerations for internal turbulent flow with incompressible fluids [65, 66].

Heat transfer and pressure drop of nanofluids

The convection heat transfer is composed of two phenomena: advection and diffusion which are related to the momentum and thermal diffusion of the flowing fluid. The values of momentum, thermal diffusions, and Prandtl number contribute to the heat transfer enhancement of the nanofluids. Figures 13 and 16 show the effect of Prandtl number on the Nusselt number at certain Reynolds number

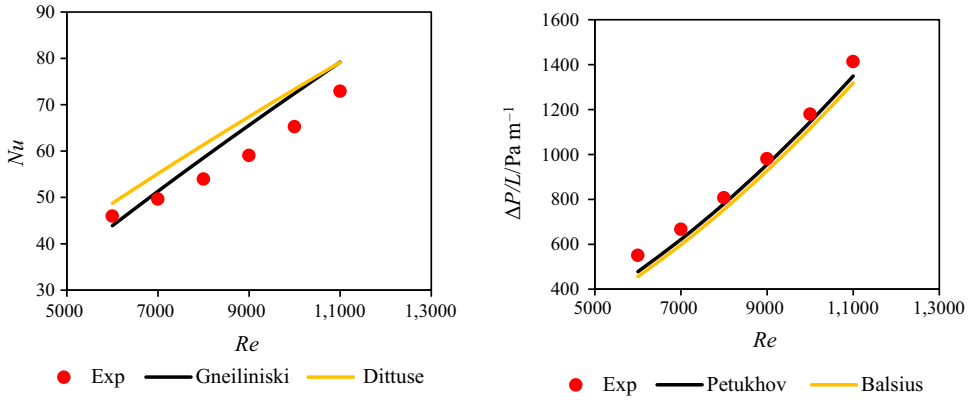

Fig. 7 Nusselt number and pressure drop profiles of the square tube with DW

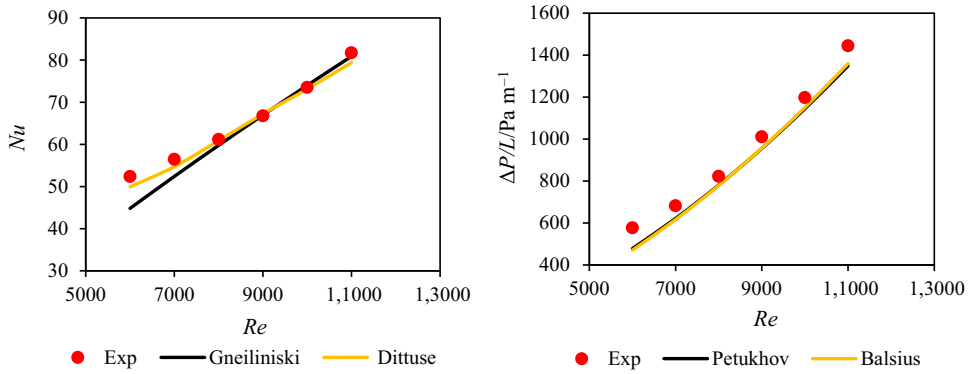

Fig. 8 Nusselt number and pressure drop profiles of the circular tube with DW

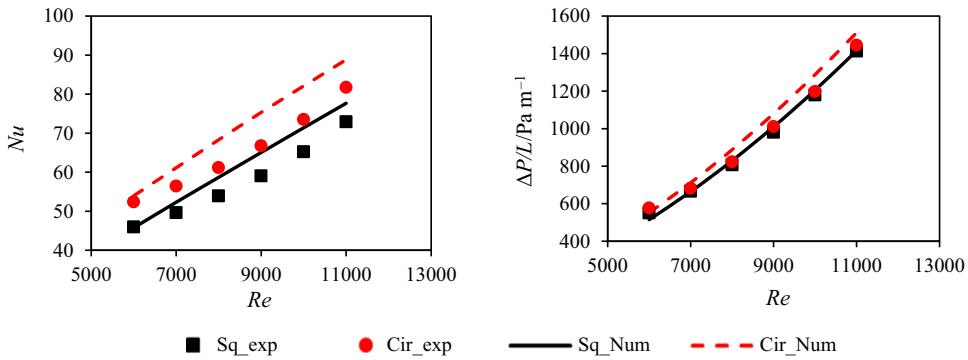

Fig. 9 Comparison between numerical and experimental results for square and circular tubes based on Nusselt number and pressure drop profiles

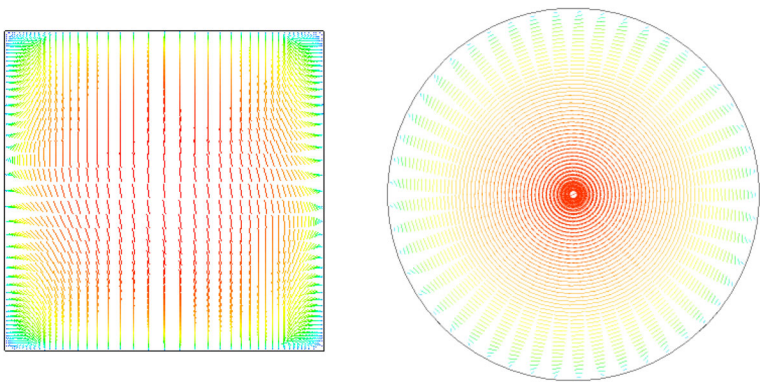

Fig. 10 Velocity profile for DW at the middle section of the square and circular tubes at Reynolds number of 6000

by using the square and circular tubes, respectively. The fluid with the highest Prandtl number has presented the highest value of the Nusselt number and the vice versa which describes why the Nusselt number is higher for the DW comparing to the KRG nanofluid. Referring to Eqs. (9) and (11), the average convection heat transfer coefficient is directly proportional to the product of Nu and thermal conductivity, and hence, the effect of the enhancement of the thermal conductivity of nanofluids will appear and it makes the trend of the average heat transfer coefficient different from those of the Nu as in the case of GNP–SDBS/DW as shown in Figs. 14 and 17 for the square circular tube, respectively. Therefore, the enhancement of convection heat transfer coefficient was not consistent with the average of Nusselt number. The momentum diffusivity has the greatest effect on the pressure drop as shown in Figs. 15 and 18, and the arrangement of pressure drop curves was similar to the arrangement of the momentum diffusivity for different types of nanofluids shown in Table 1. The results display that the percentage enhancement of convection heat transfer coefficient (the benefits of nanofluids) was different from the percentage of pressure drop increasing (the penalties). The percentages of the heat transfer enhancement of the circular tube were about 6%, 5%, 23%, and 26% for Al_2O_3–DW, SiO_2–DW, KRG, and GNP–SDBS, respectively, while the highest percentages increasing of the pressure drop were about 23%, 24%, 29%, and 123% for Al_2O_3–DW, SiO_2–DW, KRG, and GNP–SDBS, respectively. As there are penalties in the form of pressure drop side by side with benefits in the form of convection heat transfer enhancement; the performance index of each nanofluid should be presented and discussed.

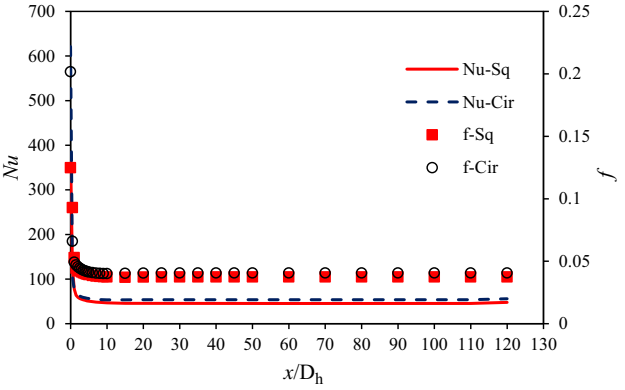

Fig. 12 Development of the Nusselt number and friction factor for DW along the tube length for both circular and square tubes at Re = 6000

The performance index is defined as the ratio of the positive enhancement (heat transfer enhancement) to the negative enhancement (pumping power increment) as shown in Eq. (24)

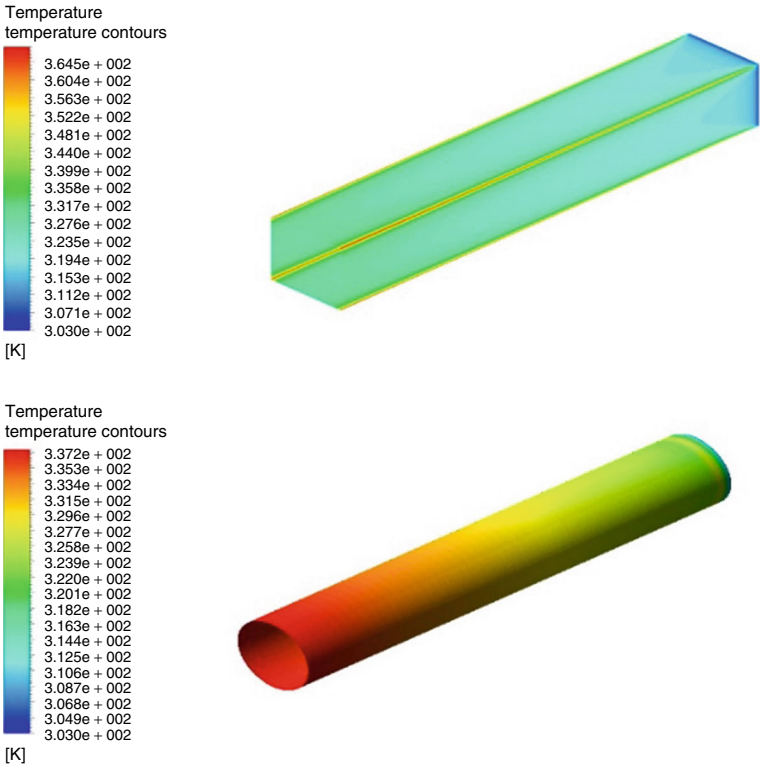

Fig. 11 Wall temperature contours for DW at Re = 6000

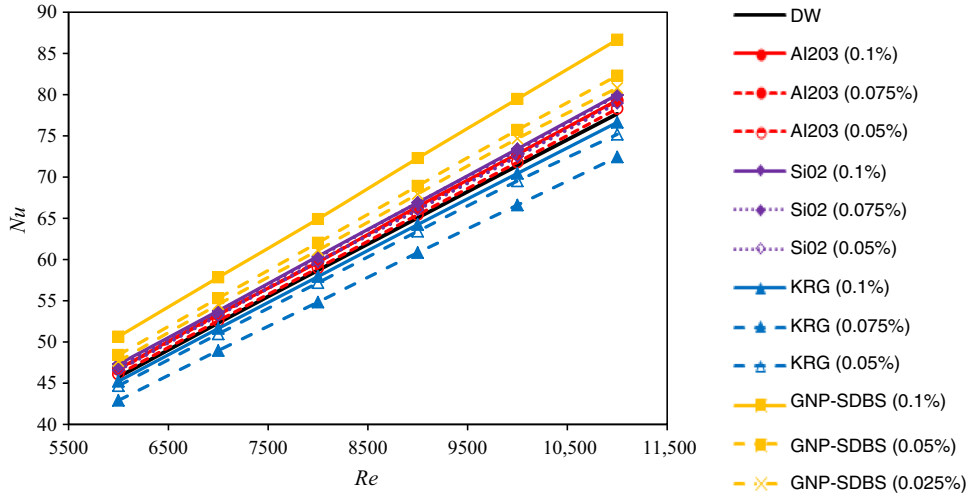

Fig. 13 Profile of average Nusselt number for DW and different nanofluids for square duct

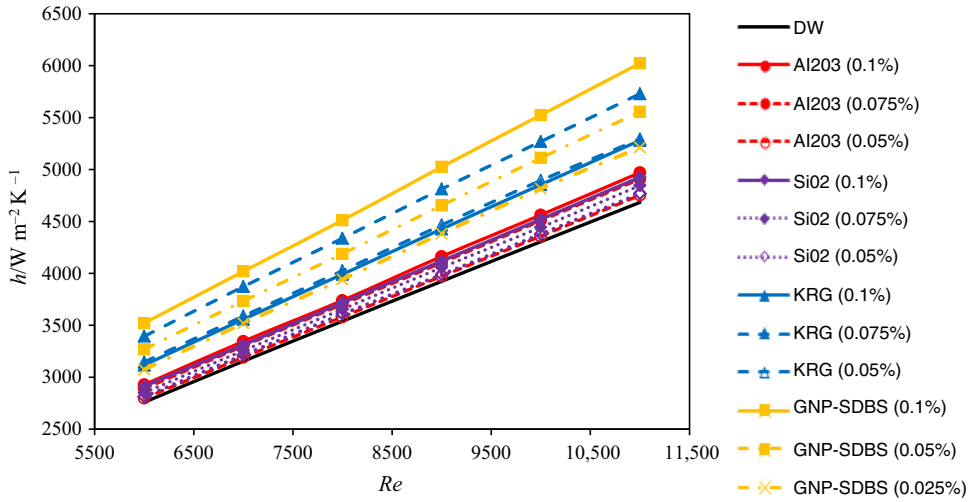

Fig. 14 Profile of average convection heat transfer coefficient for DW and different nanofluids for square duct

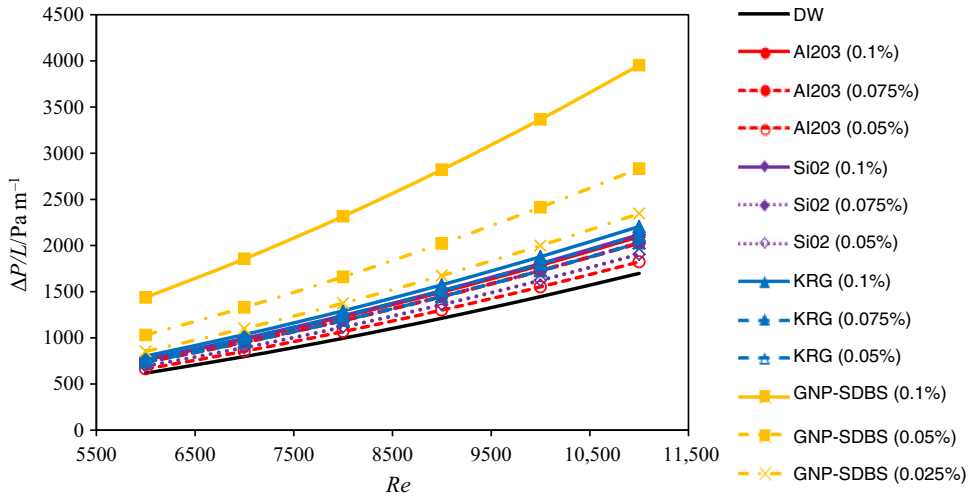

Fig. 15 Profile of pressure drop for DW and different nanofluids for square duct

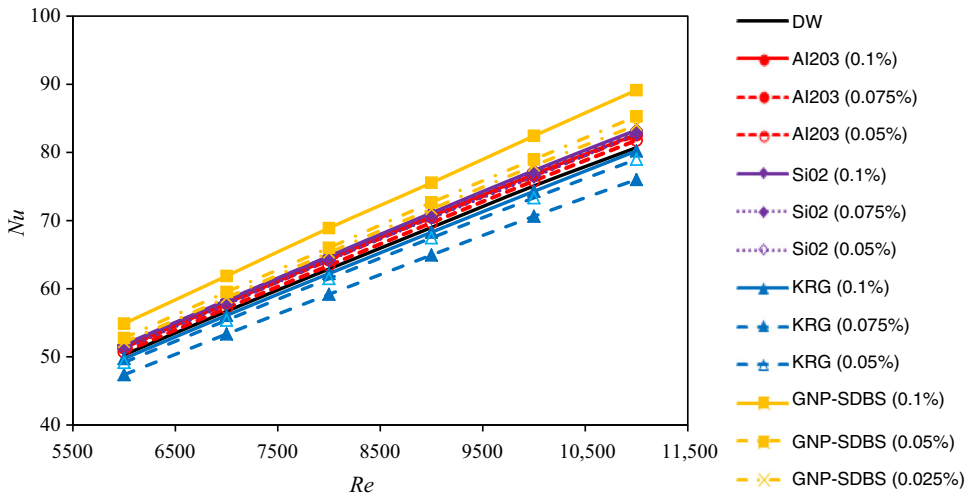

Fig. 16 Profile of average Nusselt number for DW and different nanofluids for circular tube

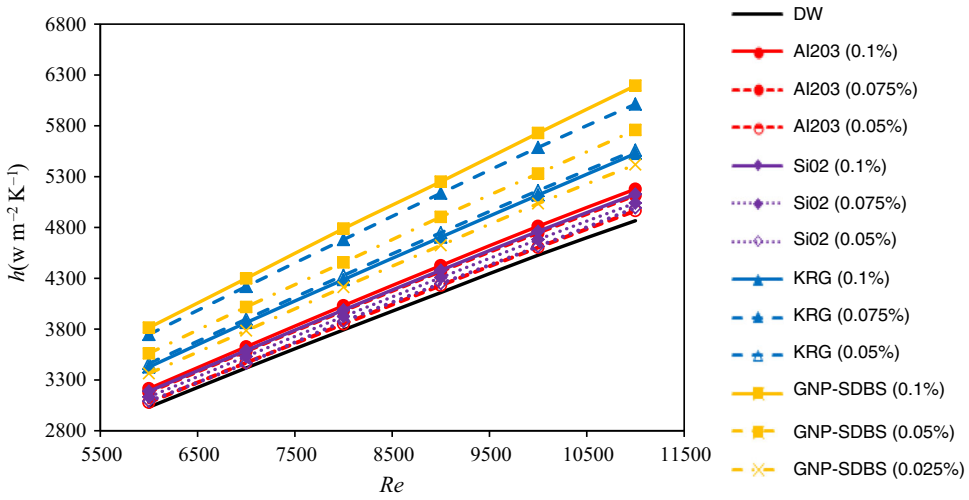

Fig. 17 Profile of average convection heat transfer coefficient for DW and different nanofluids for circular tube

$$IP = \frac{h_{nf}/h_{bf}}{\dot{W}_{nf}/\dot{W}_{bf}}. \quad (24)$$

The investigators usually adopt the pressure drop increment as a negative enhancement when calculating the performance index. In contrast, this study used the friction pumping power rather than the pressure drop due to the effect of the volume flow rate change. Figures 19 and 20 display the profile of performance index versus Reynolds number in case of circular and square ducts, respectively. Furthermore, the DW appeared to be the most efficient convective medium compared to the other nanofluids. Consequently, the consideration of the heat transfer enhancement in comparison with the pressure drop could be the critical factor in selecting the nanofluids instead of the distilled water in different heat transfer applications. For the requirement of enhanced heat transfer overruling, the pressure loss compensation nanofluids are preferred; otherwise, it would not be economic.

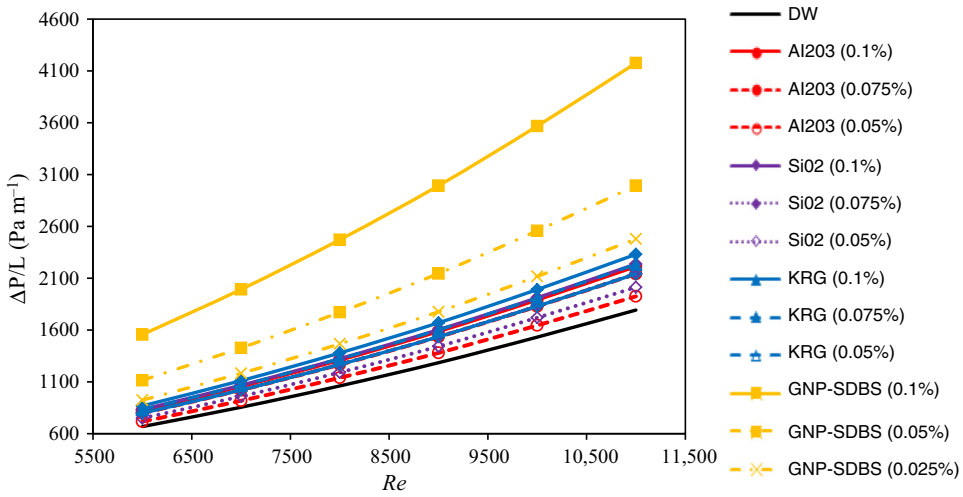

Fig. 18 Profile of pressure drop for DW and different nanofluids for circular tube

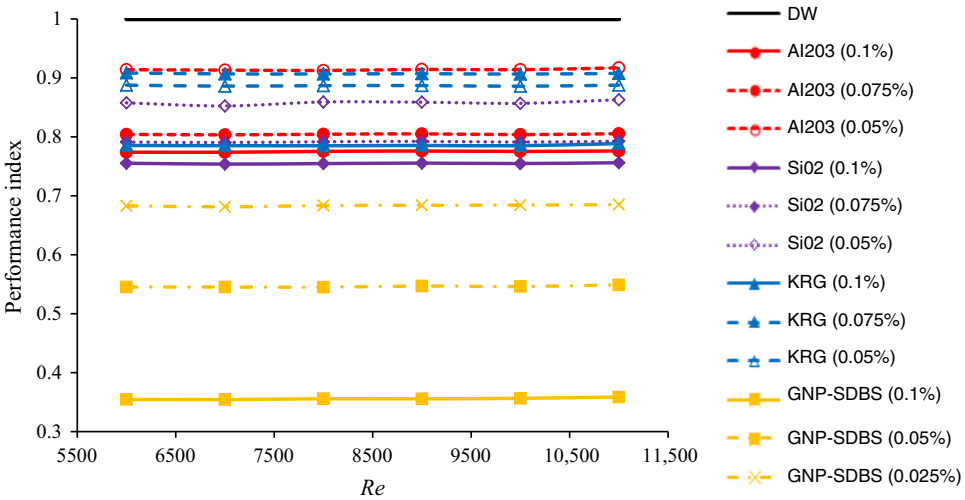

Fig. 19 Performance index based on pumping power for DW and different nanofluids for the circular tube

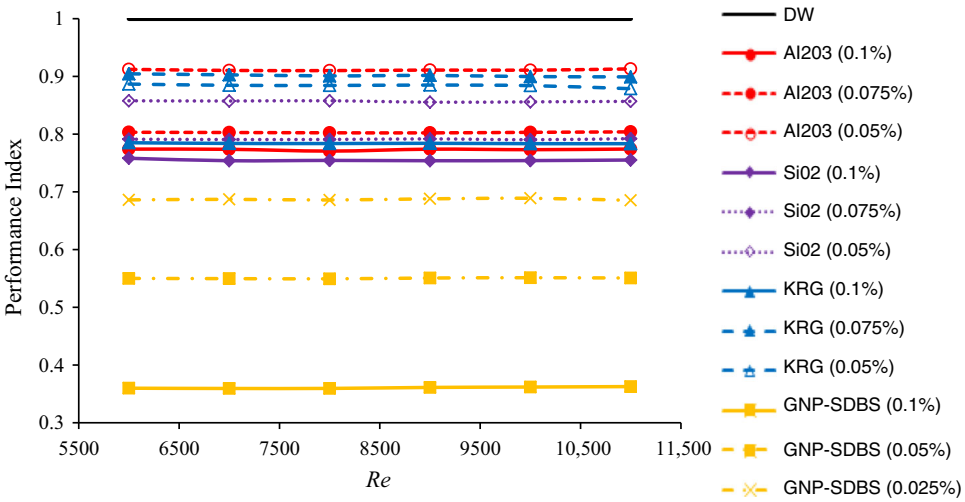

Fig. 20 Performance index based on pumping power for DW and different nanofluids for the square duct

Conclusions

The present research has focused on the effect of using metallic oxides (Al_2O_3 and SiO_2) and carbon-based nanostructures (KRG and GNP) as additives in heat transfer media for improving the turbulent convective heat transfer performance in closed conduit flow. Thermophysical properties of nanofluids were measured experimentally and theoretically to evaluate the overall heat transfer coefficient and pressure drop of samples in turbulent flow through square and circular cross-sectional tubes under constant heat flux boundary condition. The following conclusions could be drawn:

1. The mesh sizes of 384,000, 600,000, 864,000, 1,563,000, and 2,400,000 elements were examined for the numerical solution of square tube, while the mesh densities of 313,709, 583,889, 968,016, 1,337,232, and 5,476,460 elements were examined for the numerical solution of circular tube. Therefore, the mesh densities of 864,000 elements and 1,337,232 were displayed proper for the numerical solution of square and circular tubes, respectively.
2. For square duct, the Nusselt number obtained numerically showed a good agreement with the experimental data: the average error was 6.8%, and the average error for pressure drop was 2.49%. For circular tube, the average errors for of Nusselt number and pressure drop were 9.34% and 5.92%, respectively. Therefore, the numerical solution obtained by the commercial package was accepted for modelling the circular and square tube heat exchangers.
3. For turbulent flow, the variations between the flow inside the circular and square cross-sectional tubes were obtained from the sharp edge corners of the square configuration which created a secondary flow attributable to Reynolds stress gradient acting in the corner regions.
4. The DW has the highest performance index among all the tested fluids, and the lowest concentration of all the examined nanofluids (except KRG/DW) has the highest performance index for that specific nanofluid.
5. The non-covalent graphene is found not suitable for the general heat transfer application because it has a very low performance index. However, for a specific purpose where enhanced heat transfer is the main objective it could be the most preferred heat exchanging liquid.

Acknowledgements The authors gratefully acknowledge the University of Malaya Research Grant (UMRG: RP045C-17AET) and the University of Malaya Postgraduate Research Grant (PPP: PG 104-2016A) for support to conduct this research work.

References

1. Saidur R, Leong KY, Mohammad HA. A review on applications and challenges of nanofluids. Renew Sustain Energy Rev. 2011;15(3):1646–68.
2. Sarkar J, Ghosh P, Adil A. A review on hybrid nanofluids: recent research, development and applications. Renew Sustain Energy Rev. 2015;43:164–77.
3. Kleinstreuer C, Feng Y. Experimental and theoretical studies of nanofluid thermal conductivity enhancement: a review. Nanoscale Res Lett. 2011;6(1):229.
4. Kakaç S, Pramuanjaroenkij A. Review of convective heat transfer enhancement with nanofluids. Int J Heat Mass Transf. 2009;52(13–14):3187–96.
5. Trisaksri V, Wongwises S. Critical review of heat transfer characteristics of nanofluids. Renew Sustain Energy Rev. 2007;11(3):512–23.
6. Wang X-Q, Mujumdar AS. Heat transfer characteristics of nanofluids: a review. Int J Therm Sci. 2007;46(1):1–19.
7. Wen D, et al. Review of nanofluids for heat transfer applications. Particuology. 2009;7(2):141–50.
8. Yu W, et al. Review and comparison of nanofluid thermal conductivity and heat transfer enhancements. Heat Transf Eng. 2008;29(5):432–60.
9. Pendyala R, Chong JL, Ilyas SU. CFD analysis of heat transfer performance in a car radiator with nanofluids as coolants. Chem Eng Trans. 2015;45:1261–6.
10. Vajjha RS, Das DK, Ray DR. Development of new correlations for the Nusselt number and the friction factor under turbulent flow of nanofluids in flat tubes. Int J Heat Mass Transf. 2015;80:353–67.
11. Hussein AM, et al. The effect of nanofluid volume concentration on heat transfer and friction factor inside a horizontal tube. J Nanomater. 2013;2013:12.
12. Delavari V, Hashemabadi SH. CFD simulation of heat transfer enhancement of Al_2O_3/water and Al_2O_3/ethylene glycol nanofluids in a car radiator. Appl Therm Eng. 2014;73(1):380–90.
13. Mohanrajhu N, Purushothaman K, Kulasekharan N. Numerical heat transfer and pressure drop studies of turbulent Al_2O_3—ethylene glycol/water nanofluid flow in an automotive radiator tube. Appl Mech Mater. 2015;787:152–6.
14. Elsebay M, et al. Numerical resizing study of Al_2O_3 and CuO nanofluids in the flat tubes of a radiator. Appl Math Model. 2016;40(13):6437–50.
15. Hussein AM, et al. Numerical study on turbulent forced convective heat transfer using nanofluids TiO_2 in an automotive cooling system. Case Stud Therm Eng. 2017;9:72–8.
16. Ozbolat V, Sahin B. Numerical investigations of heat transfer enhancement of water-based Al_2O_3 nanofluids in a sinusoidal-wall channel. In: ASME 2013 international mechanical engineering congress and exposition. Volume 8A: Heat Transfer and Thermal Engineering (56345); 2013. p. V08AT09A051.
17. Khoshvaght-Aliabadi M, Rad SEH, Hormozi F. Al_2O_3–water nanofluid inside wavy mini-channel with different cross-sections. J Taiwan Inst Chem Eng. 2016;58:8–18.
18. Abu-Nada E, Masoud Z, Hijazi A. Natural convection heat transfer enhancement in horizontal concentric annuli using nanofluids. Int Commun Heat Mass Transf. 2008;35(5):657–65.
19. Izadi M, Behzadmehr A, Jalali-Vahida D. Numerical study of developing laminar forced convection of a nanofluid in an annulus. Int J Therm Sci. 2009;48(11):2119–29.
20. Togun H, et al. Numerical simulation of heat transfer and separation Al_2O_3/nanofluid flow in concentric annular pipe. Int Commun Heat Mass Transf. 2016;71:108–17.

21. Hu Y, et al. Natural convection in a nanofluid-filled eccentric annulus with constant heat flux wall: a lattice Boltzmann study with immersed boundary method. Int Commun Heat Mass Transf. 2017;86:262–73.
22. Hosseini M, et al. Numerical study of turbulent heat transfer of nanofluids containing eco-friendly treated carbon nanotubes through a concentric annular heat exchanger. Int J Heat Mass Transf. 2018;127:403–12.
23. Hafezisefat P, Esfahany MN, Jafari M. Erratum to: An experimental and numerical study of heat transfer in jacketed vessels by SiO_2 nanofluid. Heat Mass Transf. 2017;53(7):2407.
24. Benkhedda M, Boufendi T, Touahri S. Laminar mixed convective heat transfer enhancement by using Ag–TiO_2–water hybrid Nanofluid in a heated horizontal annulus. Heat Mass Transf. 2018;54(9):2799–814.
25. Rostamani M, et al. Numerical study of turbulent forced convection flow of nanofluids in a long horizontal duct considering variable properties. Int Commun Heat Mass Transf. 2010;37(10):1426–31.
26. Garoosi F, Rohani B, Rashidi MM. Two-phase mixture modeling of mixed convection of nanofluids in a square cavity with internal and external heating. Powder Technol. 2015;275:304–21.
27. Barik AK, Satapathy PK, Sahoo SS. CFD study of forced convective heat transfer enhancement in a 90° bend duct of square cross section using nanofluid. Sādhanā. 2016;41(7):795–804.
28. Khoshvaght-Aliabadi M, Arani-Lahtari Z. Proposing new configurations for twisted square channel (TSC): nanofluid as working fluid. Appl Therm Eng. 2016;108:709–19.
29. Hussain S, et al. Double diffusive nanofluid flow in a duct with cavity heated from below. Int J Mech Sci. 2017;131–132:535–45.
30. Izadi M, et al. Mixed convection of a nanofluid in a three-dimensional channel. J Therm Anal Calorim. 2019;136(6):2461–75.
31. Qi C, Yang L, Wang G. Numerical study on convective heat transfer enhancement in horizontal rectangle enclosures filled with Ag–Ga nanofluid. Nanoscale Res Lett. 2017;12(1):326.
32. Jalali H, Abbassi H. Numerical investigation of heat transfer by Al_2O_3–water nanofluid in square cavity. In: Design and modeling of mechanical systems—III. Cham: Springer; 2018.
33. Li Q, Xuan Y. Convective heat transfer and flow characteristics of Cu–water nanofluid. Sci China Ser E Technol Sci. 2002;45(4):408–16.
34. Fotukian SM, Esfahany MN. Experimental study of turbulent convective heat transfer and pressure drop of dilute CuO/water nanofluid inside a circular tube. Int Commun Heat Mass Transf. 2010;37(2):214–9.
35. Sajadi AR, Kazemi MH. Investigation of turbulent convective heat transfer and pressure drop of TiO_2/water nanofluid in circular tube. Int Commun Heat Mass Transf. 2011;38(10):1474–8.
36. Hemmat-Esfe M, Saedodin S, Mahmoodi M. Experimental studies on the convective heat transfer performance and thermophysical properties of MgO–water nanofluid under turbulent flow. Exp Therm Fluids Sci. 2014;52:68–78.
37. Sadeghinezhad E, et al. Experimental investigation of convective heat transfer using graphene nanoplatelet based nanofluids under turbulent flow conditions. Ind Eng Chem Res. 2014;53(31):12455–65.
38. Li Y, et al. Experimental investigation on heat transfer and pressure drop of ZnO/ethylene glycol-water nanofluids in transition flow. Appl Therm Eng. 2016;93:537–48.
39. Praveena Devi N, Srinivasa Rao C, Kiran Kumar K. Numerical and experimental studies of nanofluid as a coolant flowing through a circular tube. In: Numerical heat transfer and fluid flow. Singapore: Springer; 2019.
40. El Bécaye Maïga S, Tam Nguyen C, Galanis N, Roy G, Maré T, Coqueux M. Heat transfer enhancement in turbulent tube flow using Al_2O_3 nanoparticle suspension. Int J Numer Methods Heat Fluid Flow. 2006;16(3):275–92.
41. Shaikh S, Lafdi K. Thermal conductivity improvement in carbon nanoparticle doped PAO oil: an experimental study. J Appl Phys. 2007;101:7.
42. Bianco V, et al. Numerical investigation of nanofluids forced convection in circular tubes. Appl Therm Eng. 2009;29(17):3632–42.
43. Namburu PK, et al. Numerical study of turbulent flow and heat transfer characteristics of nanofluids considering variable properties. Int J Therm Sci. 2009;48(2):290–302.
44. Bianco V, Manca O, Nardini S. Numerical simulation of water/Al_2O_3 nanofluid turbulent convection. Adv Mech Eng. 2010;2:976254.
45. Lotfi R, Saboohi Y, Rashidi AM. Numerical study of forced convective heat transfer of nanofluids: comparison of different approaches. Int Commun Heat Mass Transf. 2010;37(1):74–8.
46. Bianco V, Manca O, Nardini S. Numerical investigation on nanofluids turbulent convection heat transfer inside a circular tube. Int J Therm Sci. 2011;50(3):341–9.
47. Keshavarz Moraveji M, Hejazian M. Modeling of turbulent forced convective heat transfer and friction factor in a tube for Fe_3O_4 magnetic nanofluid with computational fluid dynamics. Int Commun Heat Mass Transf. 2012;39(8):1293–6.
48. Naik MT, Vojkani E, Ravi G. Numerical investigation of turbulent flow and heat transfer characteristics of PGW–CuO nanofluids. Int J Min Metall Mech Eng (IJMMME). 2013;2:141–5.
49. Hejazian M, Moraveji MK, Beheshti A. Comparative study of Euler and mixture models for turbulent flow of Al_2O_3 nanofluid inside a horizontal tube. Int Commun Heat Mass Transf. 2014;52:152–8.
50. Saha G, Paul MC. Numerical analysis of the heat transfer behaviour of water based Al_2O_3 and TiO_2 nanofluids in a circular pipe under the turbulent flow condition. Int Commun Heat Mass Transf. 2014;56:96–108.
51. Abdelrazek AH, et al. A new approach to evaluate the impact of thermophysical properties of nanofluids on heat transfer and pressure drop. Int Commun Heat Mass Transf. 2018;95:161–70.
52. Sadri R, et al. CFD modeling of turbulent convection heat transfer of nanofluids containing green functionalized graphene nanoplatelets flowing in a horizontal tube: comparison with experimental data. J Mol Liq. 2018;269:152–9.
53. Ghozatloo A, Rashidi A, Shariaty-Niassar M. Convective heat transfer enhancement of graphene nanofluids in shell and tube heat exchanger. Exp Thermal Fluid Sci. 2014;53:136–41.
54. Arzani HK, et al. Experimental and numerical investigation of thermophysical properties, heat transfer and pressure drop of covalent and noncovalent functionalized graphene nanoplatelet-based water nanofluids in an annular heat exchanger. Int Commun Heat Mass Transf. 2015;68:267–75.
55. Incropera FP. Fundamentals of heat and mass transfer. Hoboken: Wiley; 2011.
56. Taylor JR. An introduction to error analysis: the study of uncertainties in physical measurements. New York: University Science Books; 1997.
57. Pak BC, Cho YI. Hydrodynamic and heat transfer study of dispersed fluids with submicron metallic oxide particles. Exp Heat Transf. 1998;11(2):151–70.
58. Xuan Y, Roetzel W. Conceptions for heat transfer correlation of nanofluids. Int J Heat Mass Transf. 2000;43(19):3701–7.
59. Launder BE, Spalding DB. Lectures in mathematical models of turbulence. London: Academic; 1972.
60. Gnielinski V. Neue Gleichungen für den Wärme- und den Stoffübergang in turbulent durchströmten Rohren und Kanälen. Forsch Ingenieurwesen A. 1975;41(1):8–16.

61. Petukhov BS. Heat transfer and friction in turbulent pipe flow with variable physical properties. In: Hartnett JP, Irvine TF, editors. Advances in heat transfer. London: Elsevier; 1970. p. 503–64.
62. Duan Z, Yovanovich MM, Muzychka YS. Pressure drop for fully developed turbulent flow in circular and noncircular ducts. J Fluids Eng. 2012;134(6):061201–061201-10.
63. Incropera FP, DeWitt DP. Fundamentals of heat and mass transfer. 5th ed. New York: Wiley; 2002.
64. Taler D. Determining velocity and friction factor for turbulent flow in smooth tubes. Int J Therm Sci. 2016;105:109–22.
65. Cengel YA. Heat and mass transfer: a practical approach. Bengaluru: McGraw-Hill; 2007.
66. Diessler RG. Analysis of turbulent heat transfer and flow in the entrance regions of smooth passages. New York: National Advisory Committee for Aeronautics: United States; 1953. p. 88.